Journal of Dental Sciences 16 (2021) 1214–1221

Available online at www.sciencedirect.com

ScienceDirect

journal homepage: www.e-jds.com

Original Article

Bone formation with functionalized 3D printed poly-ε-caprolactone scaffold with plasma-rich-fibrin implanted in critical-sized calvaria defect of rat

Min-Chia Chen [a,1], Hsien-Chung Chiu [a,1], Po-Jan Kuo [a], Cheng-Yang Chiang [a], Martin M. Fu [a], Earl Fu [b*]

[a] *Department of Periodontology, School of Dentistry, National Defense Medical Center and Tri-Service General Hospital, Taipei, Taiwan, ROC*
[b] *Department of Dentistry, Taipei Tzu Chi Hospital, Buddhist Tzu Chi Medical Foundation, New Taipei City, Taiwan, ROC*

Received 16 November 2020; Final revision received 29 January 2021
Available online 13 March 2021

KEYWORDS
Bone tissue engineering;
3-D printing scaffold;
Polycaprolactone;
Rat calvaria defect;
Platelet-rich fibrin

Abstract *Background/purpose:* Space-making is one of the essential factors for bone regeneration in severe bony defect. To test the hypothesis that an appropriately designed scaffold may be beneficial for the bone formation in defect, the new bone formed in the critical-size calvarial defect of rat was examined after implanted with a 3D-printed poly-ε-caprolactone (PCL) scaffold, retaining with and without plasma rich fibrin (PRF).
Materials and methods: Thirty-two rats were divided into four groups (control, PCL, PRF, and PCL-plus-PRF). A custom-made 3D-printed PCL scaffold, 900 μm in pore size, retaining with and without PRF, was implanted into a critical-sized calvarial defect, 6 mm in diameter. Animals were sacrificed at week-4 or 8 after implantation for assessing the new bone formation by dental radiography, micro-computed tomography (μ-CT), and histology.
Results: By radiography and μ-CT, significantly greater mineralization areas/volumes were observed in defects with 3D-printed scaffold groups compared to that without the scaffold in both two-time points. However, no advantage was found by adding PRF. Histology showed that bone tissues grew into the central zone of the critical defect when 3D-printed PCL scaffold was present. In contrast, for the groups without the scaffolds, new bones were formed mostly along defect borders, and the central zones of the defects were collapsed and healed with thin connective tissue.
Conclusion: Our results suggest that the use of a 900 μm pore size 3D-printed PCL scaffold may have the potential in facilitating the new bone formation.

* Corresponding author.
E-mail address: fuearl@gmail.com (E. Fu).
[1] Drs. Min-Chia Chen and Hsien-Chung Chiu contributed equally to this study.

https://doi.org/10.1016/j.jds.2021.01.015

Introduction

Severe bony defect in the dental, oral, and maxillofacial region is a common clinical challenge for clinicians. In order to restore the lost anatomy and function, alveolar bone augmentation is often required.[1–3] During the augmentation procedure, the space-making is one of the essential factors for bone growth.[4] Particulate bone graft is one of the materials frequently being used; however, due to its spotted nature, it is hard to maintain it in a specific shape at the augmentation site and to provide a stable volume during the healing period.[5–7] Block bone graft is better in preserving the anatomic morphology but still delicate in shaping during surgery.[8]

Three-dimensional-printed polycaprolactone (PCL) scaffold has the advantages in customizing macro-structural architecture, interconnected porosity, and channel size for nutrient diffusion.[9–13] The 3D scaffold has excellent biocompatibility,[9,14,15] and may be able to provides the necessary support and definite shape during the healing period.[7] However, previous critical size defect studies using 200–750 μm pore size PCL scaffold was not able to achieve more than 20% of the bone fill in the defect without adding mediators, bioactive agents, cells, or membrane.[16–23]

Plasma rich fibrin (PRF) is a biomaterial which can be easily obtained from patient's own blood after a process of centrifugation. PRF belongs to platelet concentrates that involve a simplified preparation.[24] Studies have shown many cytokines, and growth factors enmeshed into this fibrin network that potentially enhances bone regeneration.[25] There are several advantages compare to platelet-rich plasma in its natural structure and intact circulating cells (platelets, leukocyte, and other cells).[24] It was shown that the PRF clot stimulates proliferation and differentiation of osteoblasts *in vitro*[26–28] and bone regeneration in several clinical trials.[7,29–31] The present study therefore aimed to test the bone formation from a 900 μm pore size 3D printed PCL scaffold with plasma-rich-fibrin implanted in critical-sized calvaria defect of the rat without adding any bone graft or membrane.

Materials and methods

Fabrication of customized 3D-scaffolds

A one-shot extruder (Filabot, Barre, Milwaukee, WI, USA) was used to fabricate PCL monofilaments of a diameter 1.70 ± 0.08 mm from PCL pellets (Capa™ 6500, Perstorp Specialty Chemicals AB, Perstorp, Sweden). The specific filament diameter was required for use with a fused deposition modeling 3D-printer (Logan, Eir Biotech, Taipei, Taiwan). The average molecular weight was 50,000, and the pellets were used as they were received. Using the computer-aided-designed software (SolidWorks corp., Dassault Systemes, Waltham, MA, USA), the scaffold with 1.8 mm in height was created, while the shape were trimmed by a 6 mm diameter hole puncher (Fig. 1A). The customized PCL scaffold presented interconnection 300 μm PCL struts with the interval space of 900 μm pore size (Fig. 1). All scaffolds were soaked in alcohol for 24 h and exposed to UV radiation light (Philips, Eindhoven, Netherlands) for 4 h under ambient conditions before use.[32]

Preparation of platelet-rich fibrin

In this study, PRF was prepared as per the protocol described by Dohan et al.[24] Blood samples were collected without anticoagulants from a volunteer in 10 ml tubes and split into 1.5 ml Eppendorf tubes where 6 mm PCL scaffolds were added to the tubes and allowed to mix with the blood.[33] All tubes were then immediately centrifuged at 3000 rpm, with 1670 g force, for 10 min (CN-1040, Hsiangtai, New Taipei City, Taiwan). After processing, the PRF and the PCL-PRF complex scaffolds were incubated on ice until further required, whereas the deposits, including red blood cells, were discarded.

Animal experiment

Thirty two male Sprague–Dawley rats, eight week-old, were selected. Animals received the general anesthesia with intraperitoneal atropine (0.05 mg/kg), titetamme/zolazepam mixture (Zoletil 50, Virbac, Carros, French) (1.1 ml/100 g), and xylazine hydrochloride (Rompun, Bayer, Leverkusen, Germany) (0.05 ml/100 g, IP). After incision, a full-thickness flap was elevated, and the parietal bones were then aseptically exposed. Two circular defects were surgically created for each animal with a trephine (Komet, Hannover, Germany). Animals were divided into four defect groups, including defect control, PRF, PCL, and PCL-plus-PRF (PRF + PCL) groups (Fig. 1). During the surgery, the PCL and PRF + PCL scaffolds could be all precisely placed within the calvarial defects. In the PRF group, fibrin gel was placed as described in a previous study.[34] On weeks 4 and 8, half of the animals were sacrificed by carbon dioxide inhalation, and the skulls were excised and fixed in 4% paraformaldehyde. The specimens were prepared for dental radiography, μ-CT, and histology. All the animal protocols were approved by the Institutional Animal Care and Use Committee, National Defense Medical Center, Taipei, Taiwan (IACUC-15-323).

Dental radiography

Using a computerized imaging system (Asahi Xspot; Asahi Roentgen Ind. Co., LTD., Kyoto, Japan), all skull samples

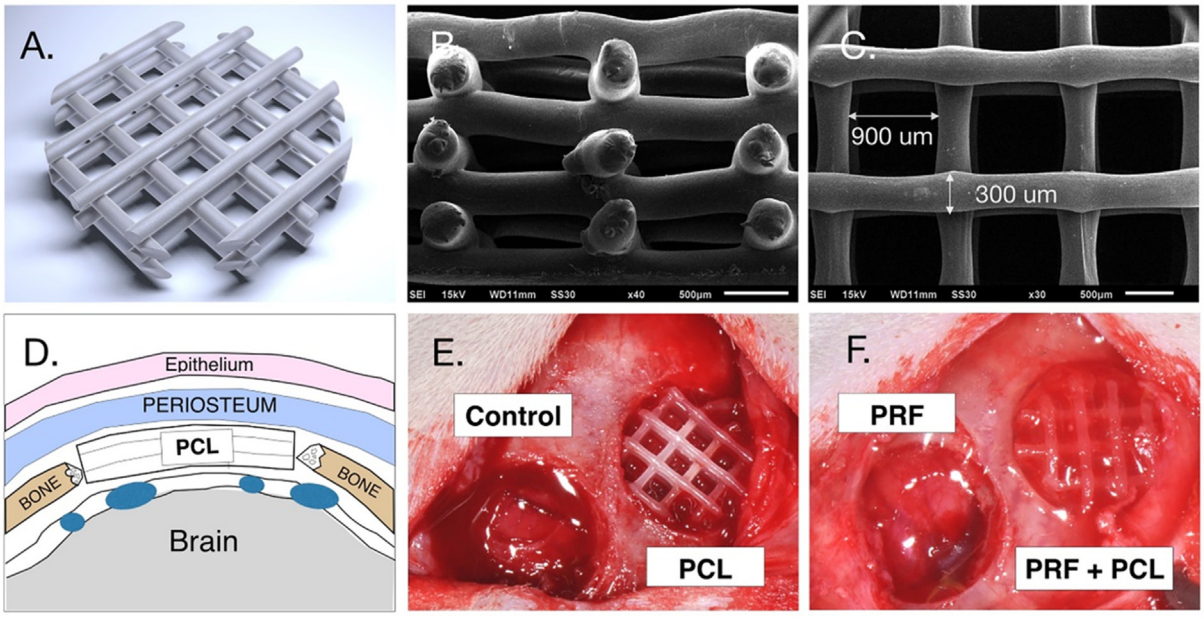

Figure 1 The computer-designed 3D-printed PCL scaffold customized for guided bone formation. (A. the scaffold, computer-designed prototype; B and C. the scaffold, the cross-sectional and vertical views, by scanning electron microscopy; D. the cartoon sculpture presenting a scaffold in the calvaria defect of the rat; E and F, the scaffolds implanted into the defects in rats) (PCL: poly-caprolactone; PRF: plasma rich fibrin; and PCF + PCL: PCL-plus-PRF).

were examined in a coronal view to determine the extent of bone formation. The X-ray tube was operated at 70 kV with a current of 6 mA for 0.12 s, at a distance 2 cm from source-to-sensor. Images were processed with the INFINITT Dental PACS image system (INFINITT North America Inc., Phillipsburg, New Jersey, USA) and the Image J processing software (National Institutes of Health, Bethesda, MD, USA).

The mean mineralized density threshold was set as a radiopaque area. In each bony defect, two zones were defined: central (<4 mm in diameter) and peripheral zones (>4 mm in diameter). Radiopaque area (mm^2) in each of the defects (<6 mm in diameter) was measured and compared among the four defect groups. The areas from two zones of every defect were also measured and compared.

Micro-computerized tomography

Using a high-resolution micro-tomography scanner (Skyscan1076, Aartselaar, Belgium), the specimens were scanned. The tube was operated at 50 kVp accelerated potential, 200 μA beam current for 460 ms, 18 μm image pixel size, and a 0.8-degree rotation step. Data was collected and reconstructed with medical image processing software (Medical image illustrator, Visualization and Interactive Media Laboratory, National Center for High-performance Computing, Taipei, Taiwan). After standardization, the coronal, axial, and sagittal slices of each defect were assessed. In the region of interest, the mineralized volume (MV) and its relative volume (MV/TV) were calculated. Among the four defect groups, the parameters recorded in each of the defects and zones were compared.

Histology and histometry

After being fixed in 10% formalin for 24 h, the parietal bones were then soaked in alcohol for sequential dehydration before embedding in resin.[35] Sixty four calvaria specimens were cut into 80-μm-thick sections in cross-sectional direction by a microtome (SP1600, Leica, Wetzlar, Germany). The slides were then stained with hematoxylin and eosin[36] and the histology characteristics were evaluated under light microscopy (DMI3000B, Leica, Wetzlar, Germany). Under the microscope, the healed fibrous tissues, bony tissues, and the residual PCL struts in the defects were compared grossly and quantitatively (histometry) among groups. The sections were cut from the middle of defects in a longitudinal direction. The healed tissue area was defined as the tissue space between the periosteum of the skin flap and the dura mater. The areas of bone, connective tissue, and residual PCL were recorded as the tissue areas in mm.[2] Besides, the percentage of each component in defect, including bone, connective tissue, and residual PCL, in the total tissue area, were also measured and recorded as a tissue area in %. The central zone was defined as the central 4 mm in diameter of the 6 mm diameter defect, whereas the peripheral zone was defined as the 2 mm ring space mesial to the defect margin (Fig. 1F).

Statistical analysis

All data were analyzed using a statistical software package (SPSS v.15.0, IBM, Chicago, IL, USA). Among the four groups, the quantitative values obtained from dental radiography, μCT, and histometry were compared by one-way ANOVA with the post hoc analysis of Duncan's test. A *p*-value of less than 0.05 was set to indicate a significant difference.

Results

Radiographic and μ-computerized tomographic observation

Well-ordered row-by-row radiopaque squares, a waffle-lattice-like feature, were observed, in the defects implanted with PCL scaffold by dental radiography, despite the observation intervals (Fig. 2). The radiopaque areas among the four defect groups were statistically indifferent if the whole defect or only the peripheral zone of the defect were measured (at both weeks of 4 and 8). However, significantly more radiopaque areas in the two groups with PCL scaffold were noted within the central zones, if compared with the groups without PCL. On the reconstructed images of μ-CT, a similar finding of the waffle-like pattern was observed in the defect groups with PCL (Fig. 3). In addition, the parallel radiolucent tunnels running through the radiopaque squares were seen. Quantitatively, significant more MV/TV was found in the central zones of the groups with PCL than those without PCL.

Histological observation and histometric analysis

In general, the defects in the groups without PCL were collapsed in central of the defect if compared to the groups with PCL when examined by histology (Fig. 4). The new bone found in the control and PRF groups were mainly located along the defect margins, which was defined as the peripheral zone in the present study. In the groups with PCL scaffold, however, new bone could be observed in the spaces in between the residual PCL struts, but not intimately contacting the PCL struts. Residual PCL struts, observed as a circle or oval shape in cross-section, could be well noticed in both PCL and PCL + PRF groups.

Histometry confirmed the finding that significantly greater tissue area in the groups with PCL than those without PCL when either the whole defect or central zone of the defect was examined in both 4 and 8 weeks (Fig. 5A). Similarly, higher percentage of bone or connective tissue area was consistently observed within the whole defects and the central zones of defects in groups with PCL than those without PCL. Compared to the absolute tissue surface area (in mm^2), however, the results from tissue areas in percentage were dissimilar (Fig. 5B). The bone and connective tissue surface areas in percentage within whole

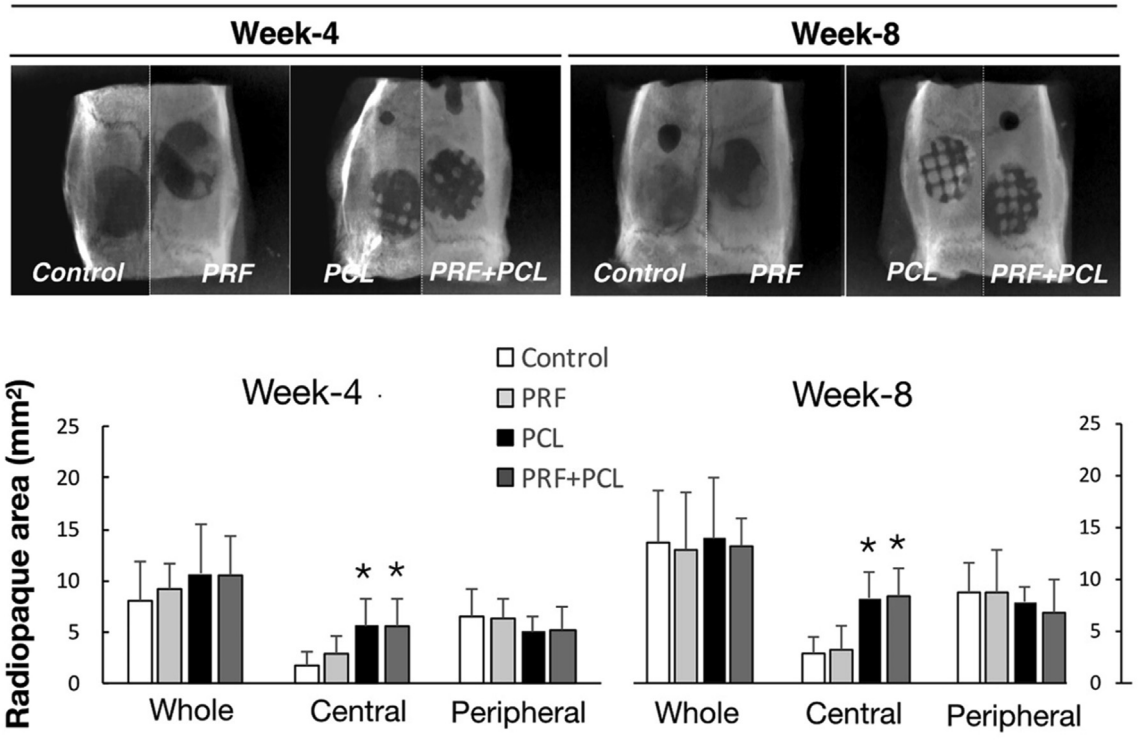

Figure 2 Radiographic evaluation of the mineralization for the 4 defect groups received with 3D-PCL scaffold and PRF. The top images are presenting the mineralization of the four defect groups (the defect control, PRF, PCL, and the PCL + PRF groups) by dental radiography at the observation intervals of weeks 4 and 8. The lower plots are showing the quantitative comparison of the radiopaque areas recorded among 4 defect groups from either the whole defects or from the divided central and peripheral zones at the week 4 and 8, respectively (Data presented as mean and SD; and *significantly difference *vs* control at $p < 0.05$).

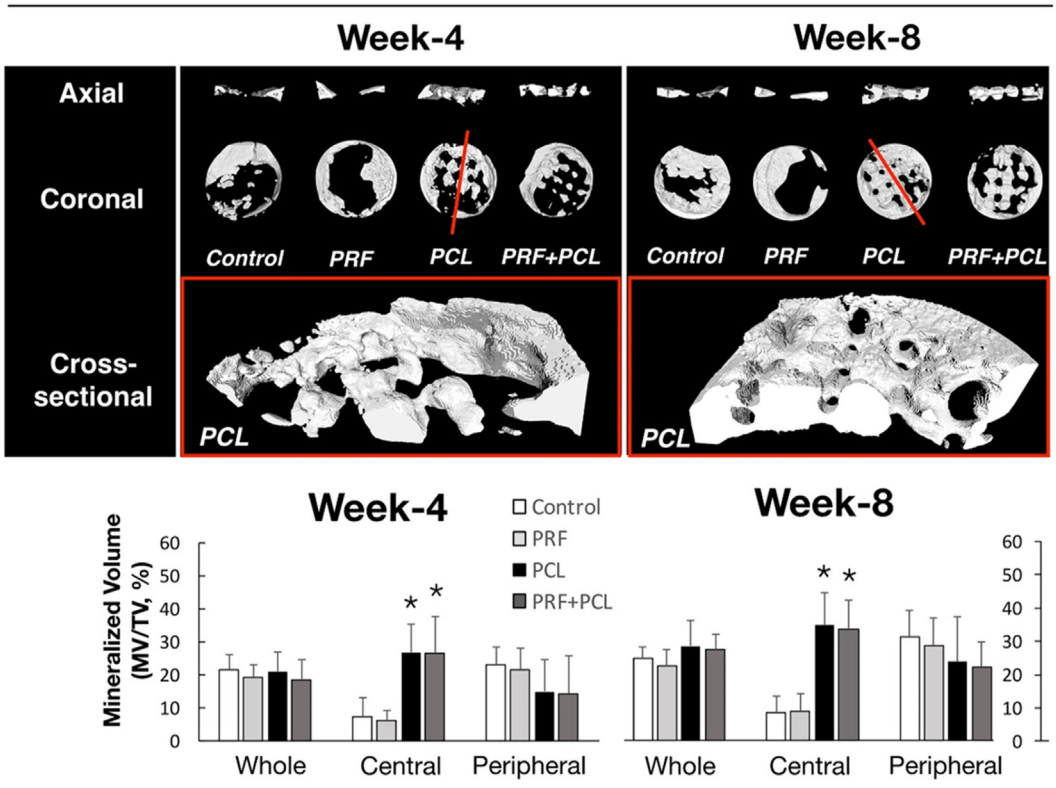

Figure 3 Tomographic evaluation of the mineralization for the four defect groups received with 3D-PCL scaffold and PRF. The top images, including the axial and coronal views, are presenting the mineralization grossly for the four defect groups (control, PRF, PCL, and the PCL + PRF) by μ-CT at the observation intervals of week 4 and 8. In contrast, the half of reconstructed images, placed in the third row, showing the mineralization at the red line cut through two images in the middle row at week-4 and -8, respectively. The bottom plots are presenting the mineralization ratios (MV/TV) in whole defects and the central and peripheral zones divided among groups (Data presented as mean and SD; and *significantly difference *vs* control at $p < 0.05$). (For interpretation of the references to color in this figure legend, the reader is referred to the Web version of this article.)

defect were statistical indifferent among the four groups; however, the higher bone areas in %, but the less connective tissue areas in %, were observed within the central zones of the PCL groups than those without PCL. In peripheral zones, the fewer bone areas in %, but the higher connective tissue areas in %, were noted in groups with PCL compared to groups without PCL (statistical difference was obtained only at week 8). The residuals of PCL were observed in defects of groups with PCL. In contrast, the measured areas in the two groups with PCL, including the absolute and relative areas, were statistically indifferent.

Discussion

In this study, 900 μm pore size 3D-printed PCL scaffolds with plasma-rich-fibrin were implanted into rat calvarial defects without adding any bone graft or membrane. After 4 and 8 weeks, new bone could be found in around 40% of the surface area in the central part of the defect when PCL scaffold was present. In contrast, mineralization only existed along the defect borders in those groups without scaffold (control and PRF groups) (Figs. 2 and 3).

In general, because 3D-printed PCL scaffold does not require additional cutting or shaping during surgery, the scaffolds simplify the bone augmentation procedure by its close fit design into the defect (Fig. 1). The 3D-customized scaffold provides a more predictable way in surgery; this advantage has been noticed in several case reports.[7,37–40]

In the present study, mineralized tissue could be easily observed in between PCL struts with dental radiographs and μ-CT after 4 and 8 weeks of healing. Mineralization appeared as the lattices and evenly distributed in defects of the scaffold groups. A particular mineralized pattern was observed in the 900 μm pore size PCL spaces. Similar designs have been done in previous studies with smaller (i.e. 200—750 μm) pore size PCL scaffold,[16–23] but minimal new bone formation or a maximum of 20% mineralization volumes could be obtained in all of those studies without adding other materials such as cells, mediators, bone grafts, or membrane. In contrast, around 40% of the surface area of the defect may be mineralized in our study using a 900 μm pore size scaffold instead. The relatively high new bone formation rate in our study was consistent with the results from a previous study showing around 30% BV/TV in porcine calvaria using a pore size of 1000 um.[18] We further demonstrated that the new bone could be formed evenly in both central and peripheral zones of the defects with the help of PCL scaffold (Fig. 5). Further study is definitely needed to explore the necessity of using such large pore

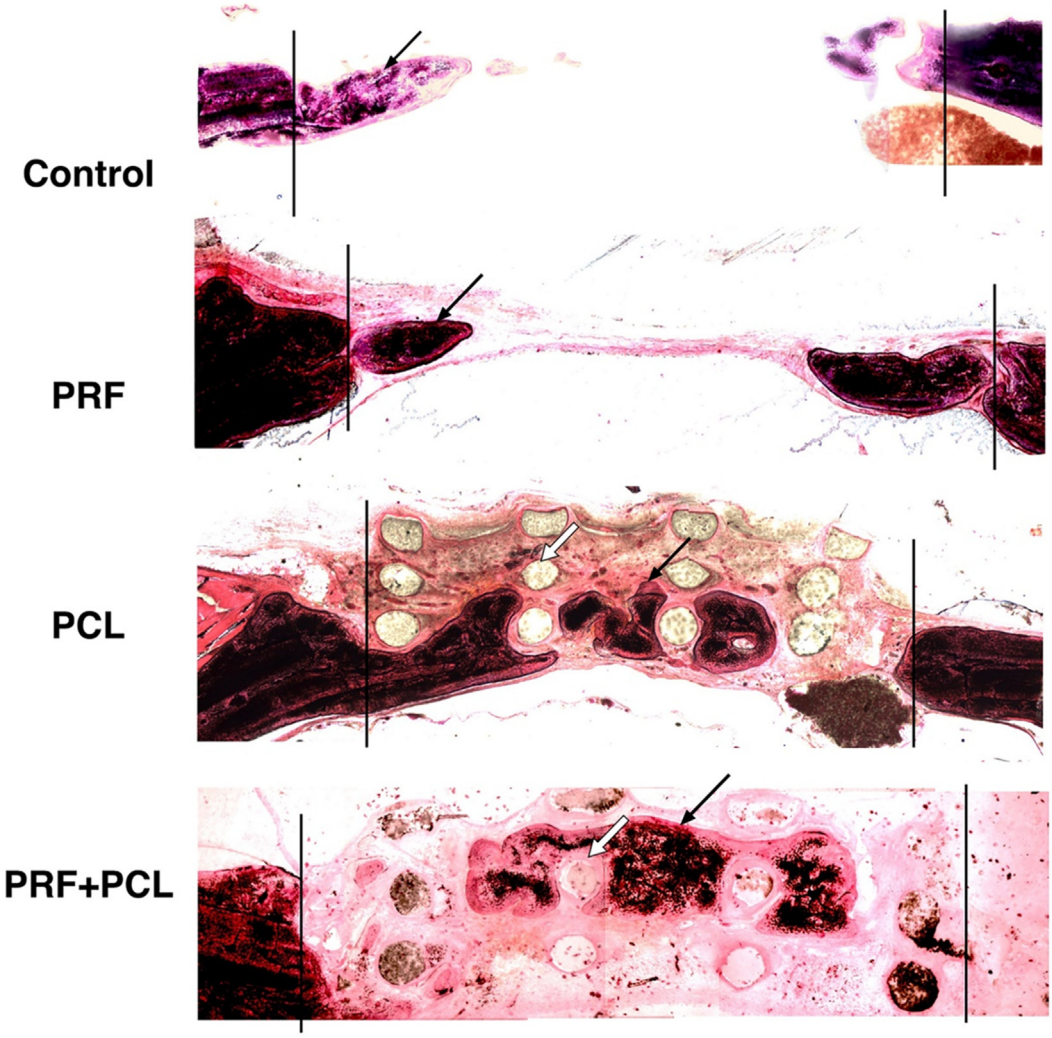

Figure 4 Histological evaluation of tissue healed in 4 defects groups received with the 3D-PCL scaffold and PRF. The histological sections were presenting the bone formation in the four calvaria defect groups, including the control, PRF, PCL, and PCL + PRF groups, respectively.

size; however, the pore size needs to be small enough to prevent tissue from collapse, but at the same time large enough to provide space for bone growth. In the small pore size scaffold, the PCL struts were designed to support, but they may further occupy the tissue spaces and let bone grow less. Therefore, an appropriate scaffold design with large enough pore size may be one of the key procedures in using the scaffold for bone tissue engineering.

In the present study, the histological finding of the newly formed bone islands between the scaffold struts confirmed that the implanted scaffold could maintain the defect volume well and might also present good compatibility with surrounding tissue (Fig. 4). However, the new bone tissues was not closely touching the strut but rather had a small distance with connective tissue in between. This finding suggests that the improvement in cell affinity with the PCL scaffold is needed.

When considering the effect of active loading agents, PRF is believed to contain numerous growth factors, such as platelet-derived growth factor, transforming growth factor, vascular endothelial growth factor, and epithelial growth factor (EGF). However, our result showed there is no significant benefit in healing rate or new bone formation ratio in 8 weeks. The details of the no significance are not known; however, the concentrations of growth factors[33] and the allogenic origins might not reach the effectiveness. Finally, likewise the bone formation, connective tissue growth into the defect space nearly to 60% of four groups (Fig. 4), which means that a barrier to prevent soft tissue invading during the early healing period may result in a better outcome.

Using a 3D-printed 900 μm pore size PCL scaffold, we demonstrated that a large pore size PCL scaffold was able to provide an architecture for new bone formation without bone graft or membrane barrier in rat critical-size calvarial defects. However, the beneficial effect of supplementary PRF was not able to be observed. Further research on the design modification of PCL and the necessity of adding

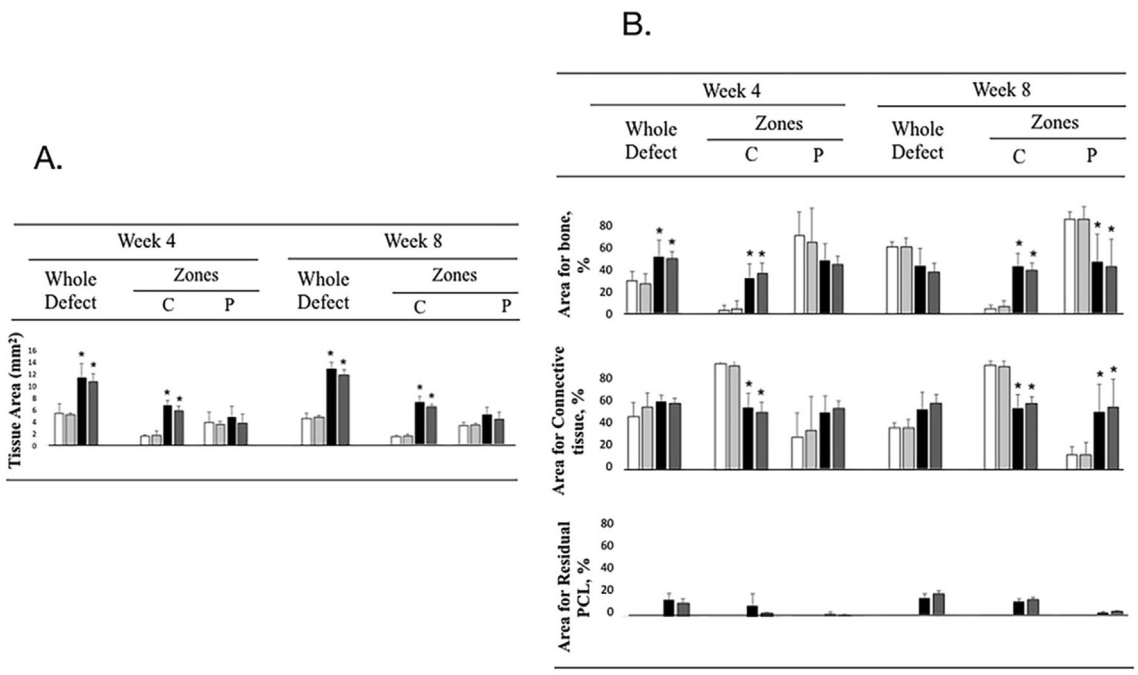

Figure 5 Histometric analysis of the tissue area. The left plot A showing the tissue area (mm^2) in the whole defects, as well as the central (C) and the peripheral (P) zones; The right plot B presenting the tissue areas in % for the bone and connective tissue, as well as the residual PCL, in the defects at the week 4 and 8. (White bar: control group, gray bar: PRF group, black bar: PCL group, and dark bar: PRF + PCL group) (*$p < 0.05$, *vs* control).

mediators or barrier membrane is still needed to find a better result of 3D-printed PCL on alveolar bone augmentation.

Authorship

Conception and design of study: Min-Chia Chen, Hsien-Chung Chiu, Cheng-Yang Chiang.

Acquisition of data: Min-Chia Chen, Po-Jan Kuo.

Analysis and/or interpretation of data: Hsien-Chung Chiu, Po-Jan Kuo, Cheng-Yang Chiang, Earl Fu.

Drafting the manuscript: Min-Chia Chen, Hsien-Chung Chiu, Cheng-Yang Chiang, Martin M. Fu, Earl Fu.

Revising the manuscript critically for important intellectual content: Min-Chia Chen, Martin M. Fu, Earl Fu.

Declaration of competing interest

The authors have no conflicts of interest relevant to this article.

Acknowledgment

The authors thank Yi-Fong Tsai for his help in the Fabrication of customized 3D-scaffolds. The research reported here was supported in part by grants from the Ministry of Science and Technology, Taiwan, ROC (MOST105-2314-B-016-020-MY2), the Ministry of National Defense Program, Taiwan, ROC (MAB-106-083) and Taipei Tzu Chi Hospital, Buddhist Tzu Chi Medical Foundation, Taiwan, ROC (TCRD-TPE-108-43).

References

1. Buser D, Bragger U, Lang NP, Nyman S. Regeneration and enlargement of jaw bone using guided tissue regeneration. *Clin Oral Implants Res* 1990;1:22—32.
2. Rocchietta I, Fontana F, Simion M. Clinical outcomes of vertical bone augmentation to enable dental implant placement: a systematic review. *J Clin Periodontol* 2008;35:203—15.
3. Lutz R, Neukam FW, Simion M, Schmitt CM. Long-term outcomes of bone augmentation on soft and hard-tissue stability: a systematic review. *Clin Oral Implants Res* 2015;26(Suppl 11):103—22.
4. Tevlin R, McArdle A, Atashroo D, et al. Biomaterials for craniofacial bone engineering. *J Dent Res* 2014;93:1187—95.
5. Troeltzsch M, Troeltzsch M, Kauffmann P, et al. Clinical efficacy of grafting materials in alveolar ridge augmentation: a systematic review. *J Craniomaxillofac Surg* 2016;44:1618—29.
6. Canullo L, Trisi P, Simion M. Vertical ridge augmentation around implants using e-PTFE titanium-reinforced membrane and deproteinized bovine bone mineral (bio-oss): a case report. *Int J Periodontics Restor Dent* 2006;26:355—61.
7. Ciocca L, Lesci IG, Mezini O, et al. Customized hybrid biomimetic hydroxyapatite scaffold for bone tissue regeneration. *J Biomed Mater Res B Appl Biomater* 2017;105:723—34.
8. Khoury F, Hanser T. Mandibular bone block harvesting from the retromolar region: a 10-year prospective clinical study. *Int J Oral Maxillofac Implants* 2015;30:688—97.
9. Hutmacher DW, Schantz T, Zein I, et al. Mechanical properties and cell cultural response of polycaprolactone scaffolds designed and fabricated via fused deposition modeling. *J Biomed Mater Res* 2001;55:203—16.

10. Izquierdo R, Garcia-Giralt N, Rodriguez MT, et al. Biodegradable PCL scaffolds with an interconnected spherical pore network for tissue engineering. *J Biomed Mater Res A* 2008;85:25—35.
11. Zein I, Hutmacher DW, Tan KC, Teoh SH. Fused deposition modeling of novel scaffold architectures for tissue engineering applications. *Biomaterials* 2002;23:1169—85.
12. Cao T, Ho KH, Teoh SH. Scaffold design and in vitro study of osteochondral coculture in a three-dimensional porous polycaprolactone scaffold fabricated by fused deposition modeling. *Tissue Eng* 2003;9(Suppl 1):S103—12.
13. Hutmacher DW. Scaffolds in tissue engineering bone and cartilage. *Biomaterials* 2000;21:2529—43.
14. Ciapetti G, Ambrosio L, Savarino L, et al. Osteoblast growth and function in porous poly epsilon-caprolactone matrices for bone repair: a preliminary study. *Biomaterials* 2003;24:3815—24.
15. Schantz JT, Teoh SH, Lim TC, et al. Repair of calvarial defects with customized tissue-engineered bone grafts I. Evaluation of osteogenesis in a three-dimensional culture system. *Tissue Eng* 2003;9(Suppl 1):S113—26.
16. Schantz JT, Hutmacher DW, Lam CX, et al. Repair of calvarial defects with customised tissue-engineered bone grafts II. Evaluation of cellular efficiency and efficacy in vivo. *Tissue Eng* 2003;9(Suppl 1):S127—39.
17. Pae HC, Kang JH, Cha JK, et al. 3D-printed polycaprolactone scaffold mixed with beta-tricalcium phosphate as a bone regenerative material in rabbit calvarial defects. *J Biomed Mater Res B Appl Biomater* 2019;107:1254—63.
18. Jensen J, Rolfing JH, Le DQ, et al. Surface-modified functionalized polycaprolactone scaffolds for bone repair: in vitro and in vivo experiments. *J Biomed Mater Res A* 2014;102:2993—3003.
19. Li J, Chen M, Wei X, Hao Y, Wang J. Evaluation of 3D-printed polycaprolactone scaffolds coated with freeze-dried platelet-rich plasma for bone regeneration. *Materials* 2017;10:831.
20. Zhang ZZ, Zhang HZ, Zhang ZY. 3D printed poly(epsilon-caprolactone) scaffolds function with simvastatin-loaded poly(lactic-co-glycolic acid) microspheres to repair load-bearing segmental bone defects. *Exp Ther Med* 2019;17:79—90.
21. Kwon DY, Kwon JS, Park SH, et al. A computer-designed scaffold for bone regeneration within cranial defect using human dental pulp stem cells. *Sci Rep* 2015;5:12721.
22. Rezai-Rad M, Bova JF, Orooji M, et al. Evaluation of bone regeneration potential of dental follicle stem cells for treatment of craniofacial defects. *Cytotherapy* 2015;17:1572—81.
23. Bae EB, Park KH, Shim JH, et al. Efficacy of rhBMP-2 loaded PCL/beta-TCP/bdECM scaffold fabricated by 3D printing technology on bone regeneration. *BioMed Res Int* 2018;2018:2876135.
24. Dohan DM, Choukroun J, Diss A, et al. Platelet-rich fibrin (PRF): a second-generation platelet concentrate. Part I: technological concepts and evolution. *Oral Surg Oral Med Oral Pathol Oral Radiol Endod* 2006;101:e37—44.
25. Kumar YR, Mohanty S, Verma M, et al. Platelet-rich fibrin: the benefits. *Br J Oral Maxillofac Surg* 2016;54:57—61.
26. Clipet F, Tricot S, Alno N, et al. In vitro effects of Choukroun's platelet-rich fibrin conditioned medium on 3 different cell lines implicated in dental implantology. *Implant Dent* 2012;21:51—6.
27. Li Q, Pan S, Dangaria SJ, et al. Platelet-rich fibrin promotes periodontal regeneration and enhances alveolar bone augmentation. *BioMed Res Int* 2013;2013:638043.
28. Lee HM, Shen EC, Shen JT, et al. Tensile strength, growth factor content and proliferation activities for two platelet concentrates of platelet-rich fibrin and concentrated growth factor. *J Dent Sci* 2020;15:141—6.
29. Mazor Z, Horowitz RA, Del Corso M, et al. Sinus floor augmentation with simultaneous implant placement using Choukroun's platelet-rich fibrin as the sole grafting material: a radiologic and histologic study at 6 months. *J Periodontol* 2009;80:2056—64.
30. Simonpieri A, Choukroun J, Del Corso M, Sammartino G, Dohan Ehrenfest DM. Simultaneous sinus-lift and implantation using microthreaded implants and leukocyte- and platelet-rich fibrin as sole grafting material: a six-year experience. *Implant Dent* 2011;20:2—12.
31. You JS, Kim SG, Oh JS, Kim JS. Effects of platelet-derived material (platelet-rich fibrin) on bone regeneration. *Implant Dent* 2019;28:244—55.
32. Braghirolli DI, Steffens D, Quintiliano K, et al. The effect of sterilization methods on electronspun poly(lactide-co-glycolide) and subsequent adhesion efficiency of mesenchymal stem cells. *J Biomed Mater Res B Appl Biomater* 2014;102:700—8.
33. Nakatani Y, Agata H, Sumita Y, Koga T, Asahina I. Efficacy of freeze-dried platelet-rich plasma in bone engineering. *Arch Oral Biol* 2017;73:172—8.
34. Kretlow JD, Spicer PP, Jansen JA, et al. Uncultured marrow mononuclear cells delivered within fibrin glue hydrogels to porous scaffolds enhance bone regeneration within critical-sized rat cranial defects. *Tissue Eng A* 2010;16:3555—68.
35. Goldschlager T, Abdelkader A, Kerr J, Boundy I, Jenkin G. Undecalcified bone preparation for histology, histomorphometry and fluorochrome analysis. *J Vis Exp* 2010;8:1707.
36. Cardiff RD, Miller CH, Munn RJ. Manual hematoxylin and eosin staining of mouse tissue sections. *Cold Spring Harb Protoc* 2014;2014:655—8.
37. Holzapfel BM, Rudert M, Hutmacher DW. Scaffold-based bone tissue engineering. *Orthopade* 2017;46:701—10.
38. Liu A, Xue GH, Sun M, et al. 3D printing surgical implants at the clinic: a experimental study on anterior cruciate ligament reconstruction. *Sci Rep* 2016;6:21704.
39. Chen X, Possel JK, Wacongne C, et al. 3D printing and modelling of customized implants and surgical guides for non-human primates. *J Neurosci Methods* 2017;286:38—55.
40. Thomas D, Singh D. 3D printing in surgery — the evolving paradigm-shift in surgical implants on demand. *Int J Surg* 2017;42:58—9.